UNIVERSITY OF CALIFORNIA SAN DIEGO

Fibroblast Mitochondria Dysfunction in Charcot Marie Tooth 2B Peripheral Sensory Neuropathy

A thesis submitted in partial satisfaction of the requirements
for the degree Master of Science

in

Biology

by

Mingzheng Hu

Committee in charge:

Professor Chengbiao Wu, Chair
Professor Gen-sheng Feng, Co-chair
Professor Enfu Hui

2021

The thesis of Mingzheng Hu is approved, and it is acceptable in quality and form for publication on microfilm and electronically.

University of California San Diego

2021

TABLE OF CONTENTS

LIST OF FIGURES

ACKNOWLEDGEMENTS

I would like to acknowledge Professor Chengbiao Wu for his support as the chair of my committee. Through multiple drafts and many long nights, his guidance has proved to be invaluable.

I would also like to acknowledge the "Yingli Gu" of Wu's Lab, without whom my research would have no doubt taken five times as long. It is their support that helped me in an immeasurable way.

The material in this thesis is currently being prepared for submission for publication. Hu, Mingzheng; Wu, Chengbiao; Gu, Yingli. The thesis author was the primary author of this material.

ABSTRACT OF THE THESIS

Fibroblast Mitochondria Dysfunction in Charcot Marie Tooth 2B
Peripheral Sensory Neuropathy

by

Mingzheng Hu

Master of Science in Biology

University of California San Diego, 2021

Professor Chengbiao Wu, Chair
Professor Gen-sheng Feng, Co-Chair

Charcot-Marie-Tooth type 2B (CMT2B) is a rare inherited autosomal dominant axonal neuropathy of the peripheral sensory system. The disease is characterized by sensory loss, muscle weakness, and atrophy in the body's periphery. Genetically, CMT2B is caused by mutation(s) in Ras-related protein Rab7, a GTP-binding protein that is fundamental for regulating endocytic pathways and trafficking. Recent studies suggested that Rab7 was also associated with mitochondria structure and function. Therefore, our group is interested in studying the link between mitochondrial morphology and the degeneration of the sensory fibers in CMT2B.

We generated a $Rab7^{V162M}$ knock-in mouse model and obtained all three genotypes: wt

(+/+), heterozygote (KI/+), and homozygote (KI/KI). I cultured mouse embryonic fibroblasts (MEFs) for all genotypes and analyzed their mitochondria morphology. I found that the mitochondria in the mutant mice were fragmented, while the wild-type mitochondria were filamentous. One potential explanation is that Rab7 mutation(s) increased dynamin-related protein 1 (DRP1) activity, a critical regulator that promotes mitochondrial fission. To test this, we found that the DRP1 inhibitor, Mdivi-1, rescued excessive mitochondrial fragmentation. Furthermore, the Rab7 inhibitor, CID, also showed a rescuing effect. We thus conclude that the CMT2B mutation(s) increased the Rab7 activity, leading to enhanced DRP1 activity. As a result, the mitochondria became extremely fragmented in CMT2B.

Introduction

Charcot-Marie-Tooth (CMT) Type 2B peripheral neuropathy (CMT2B) is an autosomal dominant disease. The onset of the disease ranges from 13-30 years (Auer-Grumbach, De Jonghe, et al., 2000; Auer-Grumbach, Wagner, et al., 2000). The patients frequently suffer from prominent neurological and muscular degenerations characterized by distal weakness and wasting, and apparent sensory loss leading to hyperkeratosis (Auer-Grumbach et al., 2003; Auer-Grumbach, De Jonghe, et al., 2000; Auer-Grumbach, Wagner, et al., 2000; Barisic et al., 2008; Bennett & Chance, 2001). In severe cases, patients develop foot ulcerations that may eventually require amputation of the distal lower limbs (Auer-Grumbach et al., 2003; Auer-Grumbach, De Jonghe, et al., 2000; Auer-Grumbach, Wagner, et al., 2000; Barisic et al., 2008; Bennett & Chance, 2001).

Mutations in Ras-related protein Rab7, a GTP-binding protein, were the causes of CMT2B (Cogli et al., 2009; Kwon et al., 1995; Meggouh et al., 2006; Verhoeven et al., 2003). Researchers have identified that there are five missense mutations at four different residues: L129F, V162M (Manganelli et al., 2012; Verhoeven et al., 2003), N161T (Houlden et al., 2004), N161I (Wang et al., 2014) and K157N (Meggouh et al., 2006). Moreover, a recent study revealed a new Rab7 variant (c.377A>G, p.K126R) in one Italian family (Saveri et al., 2020). Interestingly, unlike CMT2B patients with the five known mutations in Rab7, patients with the K126R mutation showed a predominant motor phenotype with little sensory involvement (Saveri et al., 2020).

Rab7 plays a critical role in regulating endocytic pathways (Stenmark & Gillooly, 2001; Stenmark & Olkkonen, 2001). Rab7 resides in late endosomes/lysosomes that contain many acid hydrolase enzymes (Bucci et al., 2000). By cycling between an active, GTP-bound form and an inactive, GDP-bound form, Rab7 regulates aggregation and fusion of late endosomes/lysosomes (Bucci et al., 2000). Thus, Rab7 contributes explicitly to the regulation of the cell's degradation

machinery, including the late endosomes, the lysosomes, and the autophagic vacuoles (Bucci et al., 2012; Bucci & De Luca, 2012; Bucci et al., 2000; Cogli et al., 2009; Cogli et al., 2010; Cogli et al., 2013; Colecchia et al., 2018; Liu & Wu, 2017; Zhang et al., 2013). The CMT2B-associated Rab7 mutations: L129F, V162M (Verhoeven et al., 2003), N161T (Houlden et al., 2004), and K157N (Meggouh et al., 2006), N161I (Wang et al., 2014) all occur within the highly conserved residues close to the GTP-binding pocket (Cogli et al., 2009; Cogli et al., 2010). These mutations may loosen the regulation of the GDP to GTP exchange by Rab7 guanidine-exchange factor (Rab7GEF), thus making them more prone to binding to GTP and to remain in the activated form for a prolonged period within the cell (McCray et al., 2009; Saxena et al., 2005; Spinosa et al., 2008; Zhang et al., 2013). Active Rab7 mutants result in aggregation and fusion of late endosomes/lysosomes (Bucci et al., 2000). For example, they produce enlarged endosomes in Hela cells, some as large as 10μm in diameter (Bucci et al., 2000). Furthermore, growth factor withdrawal induces activation of Rab7 that contributes to cell death (Rosales et al., 2009). Therefore, CMT2B Rab7 mutants may disrupt normal cellular trafficking, signaling, and function (Saxena et al., 2005; Spinosa et al., 2008; Zhang et al., 2013).

Rab7 plays a crucial role in regulating endocytic trafficking. Given that Rab7 is highly conserved and ubiquitously expressed in all cells, including all types of neurons (Bucci et al., 2000), it is incredibly intriguing that CMT2B-associated Rab7 mutations, except K126R (Saveri et al., 2020), appear to predominantly afflict peripheral sensory neurons in the patients (Ponomareva et al., 2016; Suter & Scherer, 2003). One plausible explanation is that these neurons tend to have extremely long axons (Bucci et al., 2012; Cogli et al., 2009; Liu & Wu, 2017), and the wellbeing of mitochondria is exceptionally critical for maintaining the structure and function of these long axons (Cogli et al., 2009; Schiavon et al., 2021; Zhang et al., 2013; Zhao et al., 2012; Zhou et al.,

2019). Thus, it is not surprising that alterations in mitochondrial motility, morphology, and function are intimately associated with CMT peripheral neuropathy (Cantarero et al., 2021). Their correlation is further evident by dominant inhibitory mutation(s) in the mitochondrial fusion protein mitofusin 2 (MFN2) (Filadi et al., 2018; Li et al., 2019) are associated with CMT2A peripheral neuropathy (Baloh et al., 2007; Fenton et al., 2021; Franco et al., 2020; Zhou et al., 2019).

Recent studies have also suggested that Rab7 plays an essential role in regulating mitochondrial structure, motility, and function(Zhao et al., 2012). Rab7 was co-immuno-precipitated with the mitochondrial fusion protein MFN2 (Zhao et al., 2012). Current studies have also indicated that Rab7 regulates phosphorylation of dynamin-related protein 1 (DRP1) (Pan et al., 2020), and increased phosphorylation of DRP1 (pS616) promotes mitochondrial fission (Galvan et al., 2019; Kim et al., 2016; Roe & Qi, 2018). Furthermore, Rab7 CMT2B mutation(s) increased tethering between lysosomes and mitochondria, leading to changes in mitochondrial morphology and reduced mitochondrial mobility (Wong, Kim, et al., 2019; Wong, Peng, et al., 2019; Wong et al., 2018). Interestingly, Rab7 is also involved in the translation of mRNAs encoding mitochondrial proteins, and CMT2B Rab7 mutation(s) markedly decreases axonal protein synthesis, impairs mitochondrial function, and compromises axonal viability (Cioni et al., 2019). These studies have provided significant insights into the potential pathogenic mechanisms by which Rab7 mutation(s) leads to peripheral sensory neuropathy in CMT2B.

However, most of the current studies employed transient overexpression of Rab7 constructs in immortal cell lines, which significantly limits the interpretation of these studies to explain the selective vulnerability of peripheral sensory neurons in human CMT2B patients. In the present study, we used fibroblasts from a $Rab7^{V162M}$ knock-in mouse model to investigate if and

how mitochondrial fragmentation in CMT2B mouse primary embryonic fibroblasts (MEFs) of the CMT2B mouse model.

Materials and Methods

Ethical Statement

All experiments involving the use of laboratory animals have been approved by the Institutional Animal Care and Use Committee of the University of California San Diego. Surgical and animal procedures were carried out strictly following the NIH Guide for the Care and Use of Laboratory Animals.

Reagents and antibodies

10x Hanks' Balanced Salt solution (HBSS), 2.5% Trypsin (10x), 100x Penicillin-Streptomycin were all purchased from Invitrogen. MEM containing GlutaMAX was from Thermal Fisher. DMEM containing high glucose (4.5g/L) was from (ThermoFisher). FBS was from Mediatech Inc (Cat# 35-010-CV). 0.1% Poly-L-Lysine (Cultrex® Poly-L-Lysine) was from Trevigen (Gaithersburg, MD; Cat# 3438-100-01). All other chemicals and lab wares were from Bio-Rad, Fisher, Sigma, VWR.

Mito Tracker™ Red FM (ThermoFisher, Cat#M22425) was purchased from Invitrogen (Carlsbad, CA).

Mdivi-1 was purchased from MedChemExpress (Cat# HY-15886). CID 11067700 was from Sigma.

Rab7^{V162M} knock-in mouse model

We have made a knock-in mouse model (C57BL6) for CMT2B by changing 484G to A (V162>M) in Rab7 Exon 5. We introduced the mutated allele into the mouse genome, together with the selection marker NeoR and two LoxP sites. The LoxP sites will facilitate studies in which selective deletion of the mutated allele is needed using Cre. We test their genotypes using the PCR primer pair. The wt gives rise to a 373 bp fragment while the mutant allele (Rab7V162M: Neo)

produces a 490 bp. We obtained all three genotypes: wt (+/+), heterozygote (KI/+), and homozygote (KI/KI) with a typical Mendelian segregation ratio. Both the KI/+ and KI/KI pubs survive to full adulthood.

Skin fibroblasts culture and maintenance

Abdominal skin tissue was dissected from wild-type, $Rab7^{V162M/+}$ heterozygous, and $Rab7^{V162M/V162M}$ homozygous E18 mouse embryos. Then the tissue was cut with scissors into about $1\times1mm^2$ small pieces. Following quick rinses in HBSS with 1% P/S, the skin tissue was dissociated in 0.25% Trypsin with mg/ml collagenase at 37℃ for 30 mins. And then, DNase I (1 mg/ml, final concentration) was added to skin tissue. Fibroblasts were isolated and loaded in the plating medium (High glucose DMEM with 15% FBS, 1% P/S). Half of the medium was replaced the following day and then every other day until the conclusion of the experiments.

Measurement of mitochondrial morphology and movement

Mito Tracker™ Red FM was diluted into MEM. Skin fibroblasts were treated with a final concentration of 50 nM of Mito Tracker at 37℃ for 30 mins. After quick rinses, the cultures were imaged live under a 63X objective lens with a zoom 1.6X using a Leica DMi8 Live Imaging Microscope. The analysis and quantification of mitochondrial morphology were carried out as described previously (Valente et al., 2017).

Mdivi-1 treatment

For fibroblasts treatment, Mdivi-1 was diluted into high-glucose DMEM to the final concentration of 50 μM and applied to $RAB7^{V162M/V162M}$ fibroblast cultures. After incubation at 37℃ for 30 mins, fibroblasts were treated with Mito Tracker ™ Red FM and live imaging as described above.

CID1067700 treatment

CID1067700 was diluted into high-glucose DMEM and applied to RAB7$^{V162M/V162M}$ fibroblast cultures at the final concentration of 1 μM and 10 μM. After incubation at 37℃ for 30 mins, fibroblasts were treated with Mito Tracker ™ Red FM and live-imaging. DMSO (1%, final concentration) was applied to the medium as the control treatment.

Quantification of mitochondrial size, network

We used the Mitochondria Analyzer plugin in ImageJ for mitochondrial analysis. First, each image was classified into different levels of fragmentation according to the visual perception (**Figure 1A**) because even the same genotype fibroblasts had a variance in their degree of fragmentation.

Then, we used the 2D Optimize Threshold command to determine the optimal parameters for samples under different conditions. Blocking size of 1.05/1.25/1.45 microns and C-value of 5/9/13 were applied for level 1, level 2, and level 3, respectively. The block size relates to the size of the object of interest, while the C-value helps remove noise and subtract background (Chaudhry et al., 2020). Next, we used the Threshold command to threshold each image based on the corresponding parameters and used the Analysis command to analyze the binary images per mitochondrion basis. The area was measured in μm^2, which revealed the size of the mitochondrion. The aspect ratio was calculated as the ratio of maximal over minimal diameter (length over width), which reflected its shape. Branch junctions (**Figure 1B**) represented the points where two or more branches in the mitochondrion's skeleton connect (Chaudhry et al., 2020). The number of branch junctions reflected the complexity of the mitochondria network.

Note that only mitochondria larger than 100/70/40-pixel units were considered in those three conditions, respectively, to remove noise further. Finally, plot the averaged area, aspect ratio,

and the number of branch junctions per mitochondrion for each genotype and plot the frequency distribution for each characteristic of the three different genotypes.

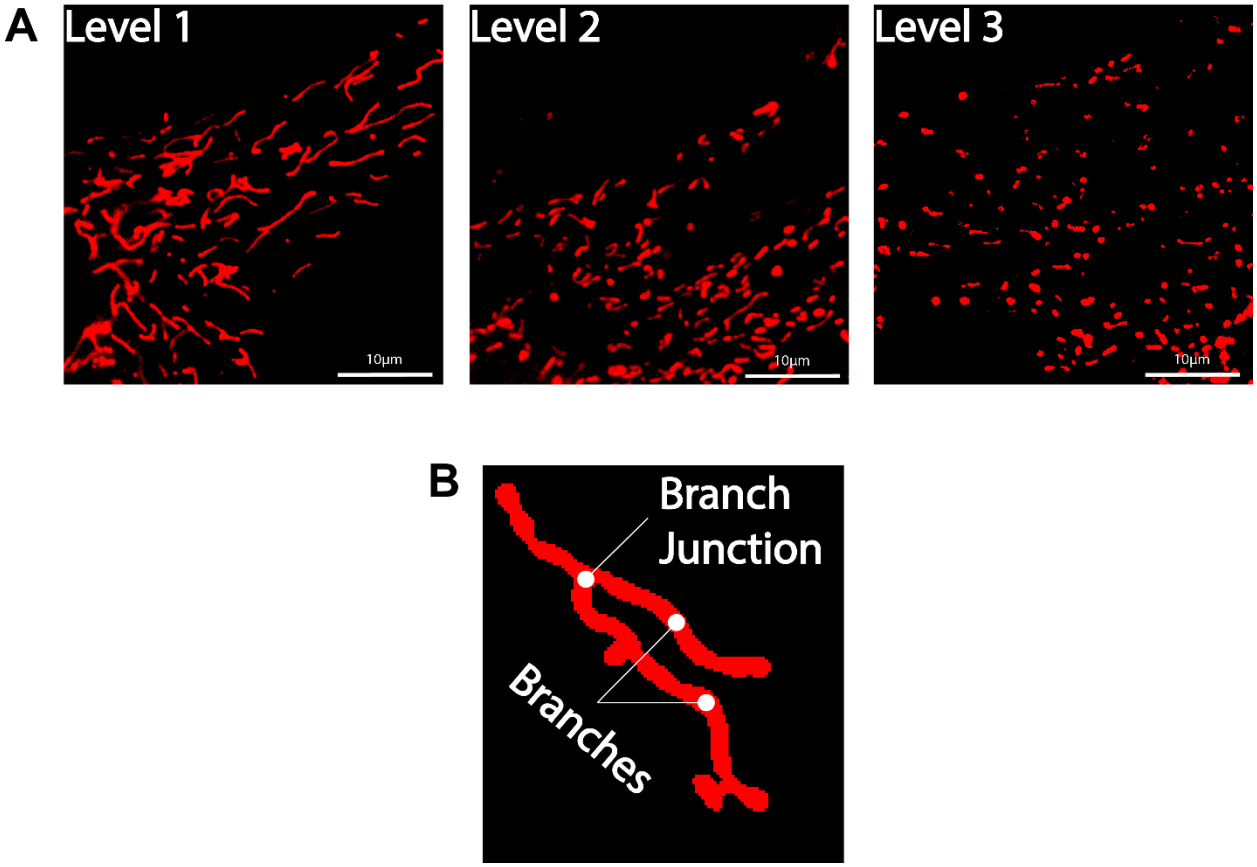

Figure 1. Illustration of different levels of fragmentation and example of branch junctions.

A. Level 1 of fragmentation, most of the mitochondria were filamentous and almost no fragmentation.
   Level 2 of fragmentation, some mitochondria were tubular, while others were dotted.
   Level 3 of fragmentation, most of the mitochondria were fragmented, the highest level of fragmentation.
B. Here are examples of branches and branch junctions.

Statistical analysis

One-way ANOVA was used to determine any significant differences between means of three or more groups. We presented the population means with the standard errors of the mean, shown as Mean ± SEM.

Results:

A. Mitochondria morphology in different genotypes

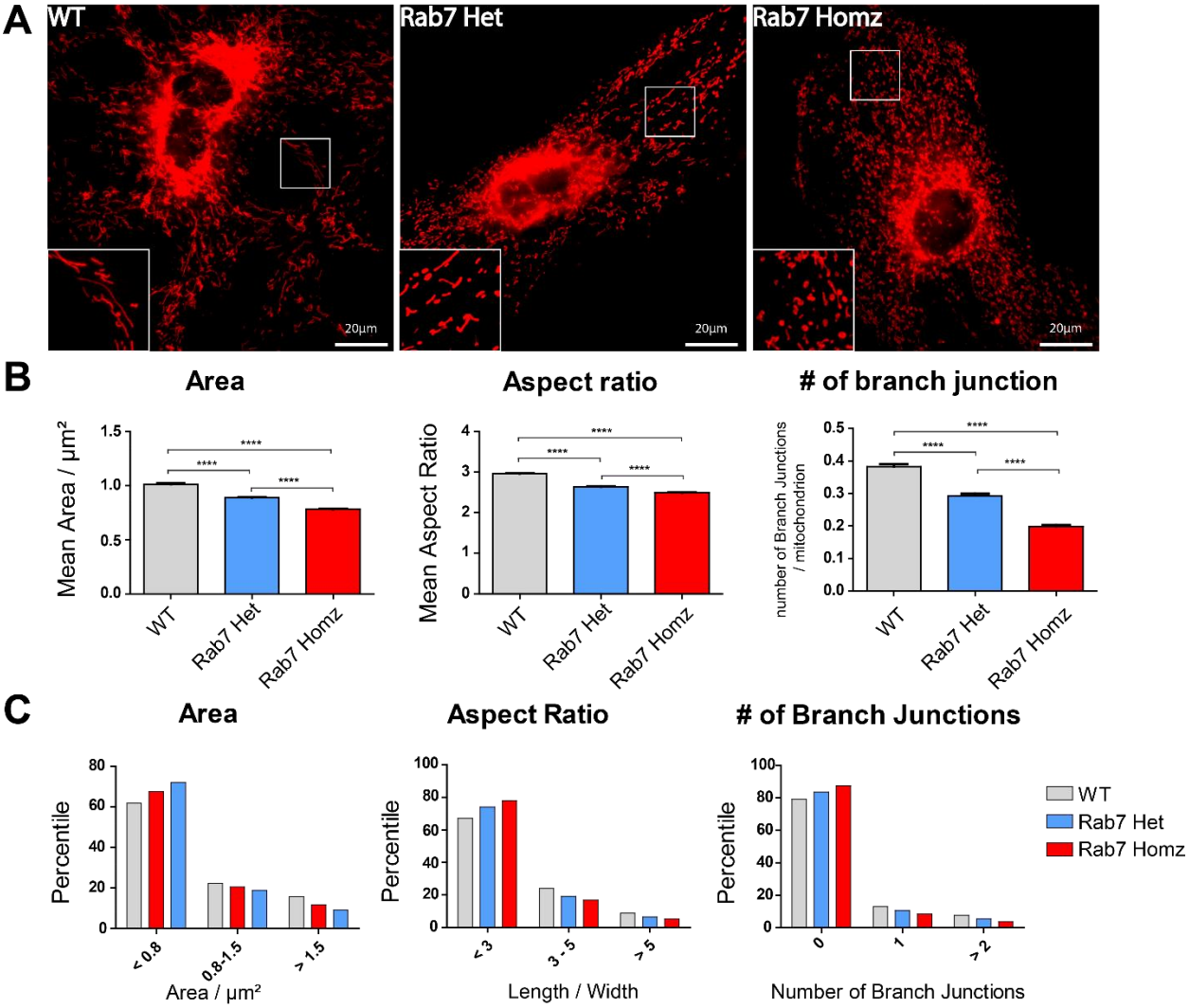

Figure 2. Mitochondria morphology for all three genotypes.

A. Here are the raw images for the three genotypes taken under live imaging microscopy. We adjust the brightness and contrast to distinguish the fluorescent signal from its background.
B. Quantification and comparison of the mean area, aspect ratio, and the number of branch junctions per mitochondrion for the three genotypes. The significant differences between groups were shown, with P-values less than 0.0001. There were 46 images for wild-type, 40 images for Rab7$^{V162M/+}$ heterozygote, and 47 images for Rab7$^{V162M/V162M}$ homozygote.
C. Here are the frequency distributions of the area, aspect ratio, and the number of branch junctions per mitochondrion. There were 23,250 mitochondria involved in wild-type, 22,947 in the Rab7$^{V162M/+}$ heterozygote, and 28,936 in the Rab7$^{V162M/V162M}$ heterozygote.

For mitochondria size and shape, we observed that the mitochondria in wild-type MEFs were generally larger and more filamentous/tubular. In comparison, the mitochondria in Rab7$^{V162M/V162M}$ homozygous MEFs were usually smaller and more fragmented/dotted. The size and shape of mitochondria in Rab7$^{V162M/+}$ heterozygous MEFs were in the middle of them (**Figure 2A**). The quantification after ImageJ processing was consistent with the visual perception. The wild-type mitochondria had the largest mean area (1.0136 ± 0.0081) and mean aspect ratio (2.9601 ± 0.0119). In contrast, the Rab7$^{V162M/V162M}$ homozygous mitochondria had the smallest (0.7823 ± 0.0049 for the mean area; 2.4908 ± 0.0085 for the mean aspect ratio), and the Rab7$^{V162M/+}$ heterozygous mitochondria had the medium size and shape (0.8898 ± 0.0072 for the mean area; 2.6310 ± 0.0104 for the mean aspect ratio; **Figure 2B**). All the differences were significant, with P-values less than 0.0001.

As for the mitochondrial network, it was difficult to identify their differences visually, so we chose a characteristic, the number of branch junctions per mitochondria, to reflect the complexity of the mitochondria network. A more significant number of branch junctions per mitochondrion indicated a more complex network and vice versa (**Figure 1B**). We found that the number of branch junctions per mitochondrion was greater in wild-type mitochondria (0.3828 ± 0.0078) and smaller in Rab7$^{V162M/V162M}$ homozygous and Rab7$^{V162M/+}$ heterozygous mitochondria (0.1987 ± 0.0042 for homozygote; 0.2931 ± 0.0067 for heterozygote; **Figure 2B**). The result indicates that mitochondria in the wild-type fibroblasts formed more complex networks, while the mitochondria in the homozygous or heterozygous fibroblasts formed less complicated networks. All the differences were significant, with P-values less than 0.0001.

To further demonstrate mitochondria morphology, we plot the distribution of the area, aspect ratio, and the number of branch junctions for all the mitochondria in each genotype. We

analyzed their frequency distribution because there was a variance within each genotype, which means not all the wild mitochondria were perfectly filamentous, and not all the mitochondria in homozygote were perfectly dot-like. The frequency distribution plot was consistent with our earlier results.

In terms of their size, the wild-type MEFs had a higher percentage of relatively large mitochondria (area > 0.8 μm^2). In comparison, $Rab7^{V162M/V162M}$ homozygote and $Rab7^{V162M/+}$ heterozygote had a higher percentage of relatively smaller mitochondria (area < 0.8 μm^2; left panel in **Figure 2C**). As for their shape, the wild-type MEFs had a higher percentile of relatively more filamentous mitochondria (aspect ratio > 3). In contrast, $Rab7^{V162M/V162M}$ homozygote and $Rab7^{V162M/+}$ heterozygote had a higher percentile of relatively more fragmented mitochondria (aspect ratio < 3; middle panel in **Figure 2C**). In addition, the wild-type MEFs had a higher proportion of branched mitochondria (≥1 branch junctions), while the $Rab7^{V162M/V162M}$ homozygote and $Rab7^{V162M/+}$ heterozygote had a higher proportion of unbranched mitochondria (0 branch junction; right panel in **Figure 2C**).

B. Mutant Rab7 led to mitochondria fragmentation by enhancing DRP1 activity.

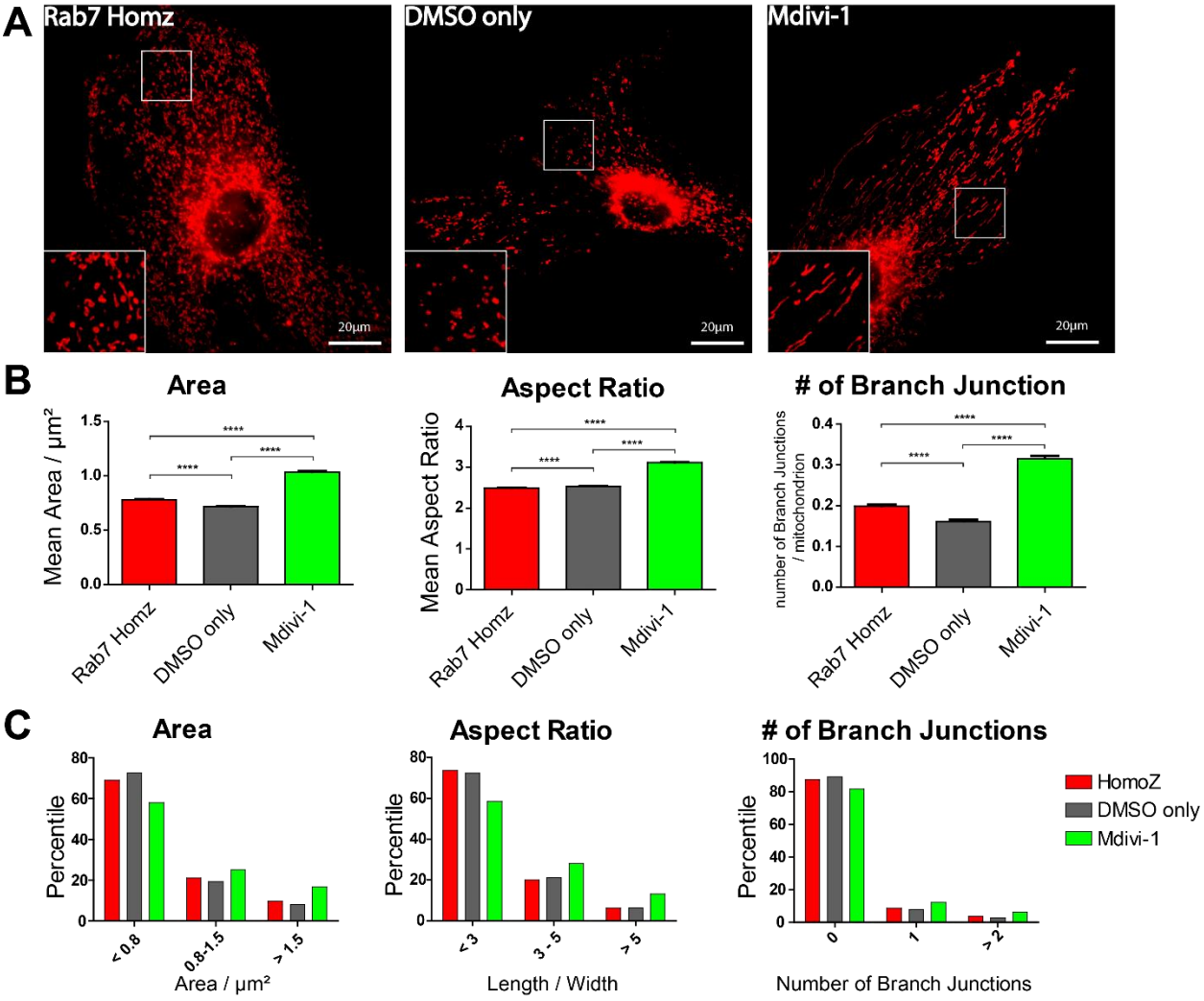

Figure 3. Mitochondria morphology for Mdivi-1 treatment.

A. Here are raw images for Rab7$^{V162M/V162M}$ homozygote, DMSO only, and Mdivi-1 treatment, taken under live imaging microscopy. We adjusted the brightness and contrast to distinguish the fluorescent signal from its background.
B. Quantification and comparison of the mean area, aspect ratio, and the number of branch junctions per mitochondrion for the three groups. The significant differences between them were shown, with P-values less than 0.0001. There were 47 images for Rab7 homozygote, 34 images for DMSO only, and 40 images for Mdivi-1 treatment.
C. Here are frequency distributions of the area, aspect ratio, and the number of branch junctions per mitochondrion. There were 28,936 mitochondria involved in Rab 7 homozygote, 28,050 in DMSO only, and 23,251 in Mdivi-1 treatment.

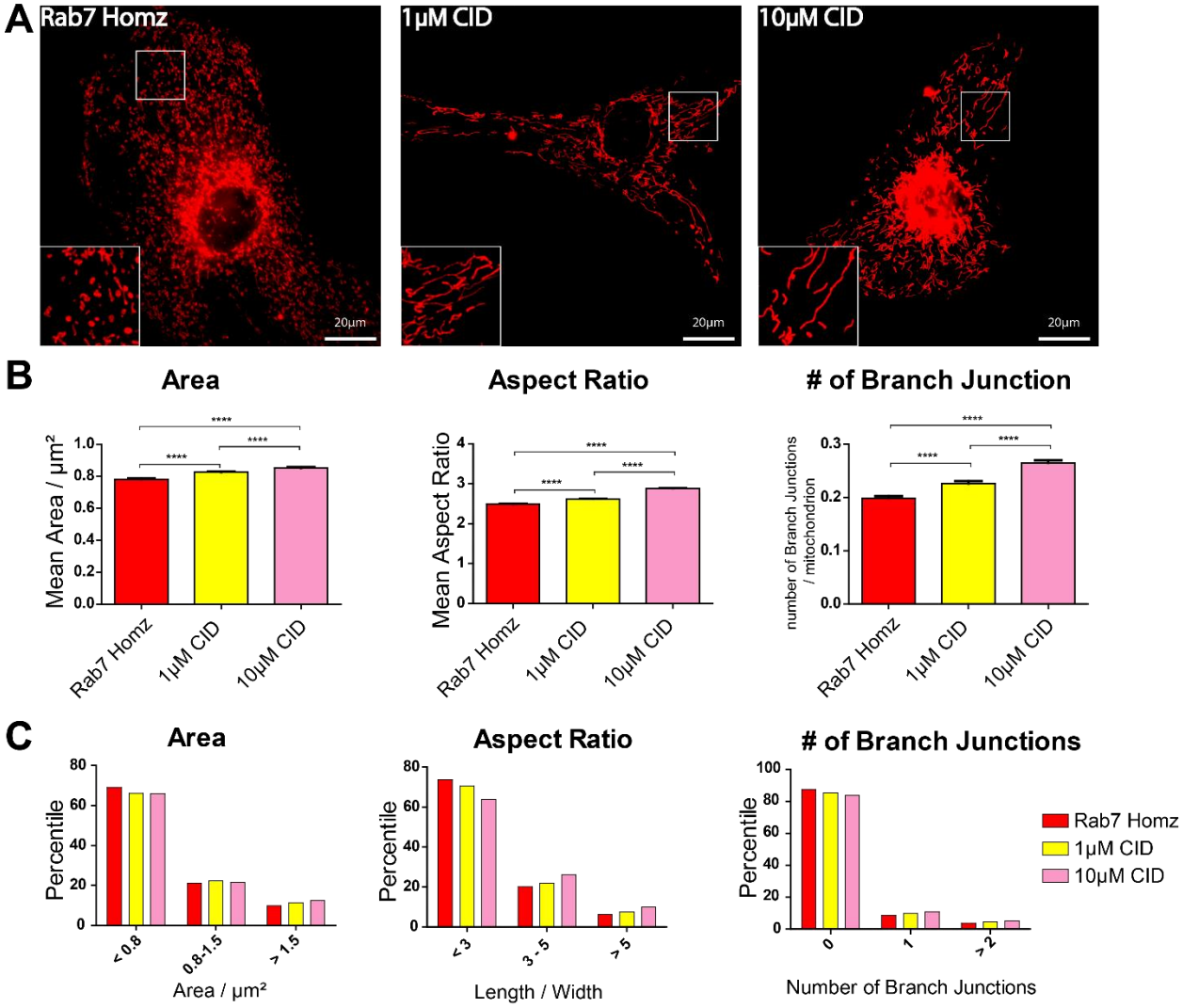

Figure 4. Mitochondria morphology for CID treatment.

A. Here are raw images for Rab7$^{V162M/V162M}$ homozygote, 1 μM CID, and 10 μM CID treatment, taken under live imaging microscopy. We adjusted the brightness and contrast to distinguish the fluorescent signal from its background.
B. Quantification and comparison of the mean area, aspect ratio, and the number of branch junctions per mitochondrion for the three groups. The significant differences between them were shown, with P-values less than 0.0001. There were 47 images for Rab7$^{V162M/V162M}$ homozygote, 36 images for 1 μM CID treatment, and 40 images for 10 μM CID treatment.
C. Here are frequency distributions of the area, aspect ratio, and the number of branch junctions per mitochondrion. There were 28,936 mitochondria involved in Rab7$^{V162M/V162M}$ homozygote, 22,628 in 1 μM CID treatment, and 28,247 in 10 μM CID treatment.

After determining the mitochondrial fragmentation in CMT2B, we were interested in how Rab7 mutation in CMT2B led to mitochondria fragmentation. Recent studies showed that the knocking down of Rab7 decreased DRP1 phosphorylation and thus decreased DRP1 activity to induce mitochondria fission (Pan et al., 2020). These studies revealed the ability of Rab7 to regulate DRP1 activity for mitochondria dynamics. Therefore, we expected that the CMT2B mutation(s) increased Rab7 activity, leading to enhanced DRP1 activity, and the elevated DRP1 activity led to excessive mitochondrial fragmentation in CMT2B. To test that, we first treated $Rab7^{V162M/V162M}$ homozygous fibroblasts with a Drp1 inhibitor, Mdivi-1, and see whether it can rescue their mitochondrial morphology.

Visually, Mdivi-1 treated mitochondria were more filamentous than $Rab7^{V162M/V162M}$ homozygous mitochondria (**Figure 3A**); statistically, the mean area, aspect ratio, and the number of branch junctions per mitochondrion were all increased significantly after Mdivi-1 treatment (for area: 1.0352 ± 0.0083 after treatment > 0.7823 ± 0.0049 before treatment; for aspect ratio: 3.1167 ± 0.0125 after treatment > 2.4908 ± 0.0085 before treatment; for number of branch junctions: 0.3155 ± 0.0063 after treatment > 0.1987 ± 0.0042 before treatment; **Figure 3B**). All the differences were significant, with P-values less than 0.0001.

Furthermore, we treated the $Rab7^{V162M/V162M}$ homozygous fibroblasts with Rab7 inhibitor CID. We tested two different concentrations of the CID: 1 μM (low) and 10 μM (high). The mitochondria were also visually more filamentous after either low or high concentration CID treatment (**Figure 4A**) and the mean area, aspect ratio and number of branch junctions per mitochondrion were also increased to a certain extent (for area: 0.8532 ± 0.0054 in high concentration > 0.8267 ± 0.0058 in low concentration > 0.7823 ± 0.0049 before treatment; for aspect ratio: 2.8844 ± 0.0101 in high concentration > 2.6205 ± 0.0102 in low treatment > 2.4908

± 0.0085 before treatment; for number of branch junctions: 0.2648 ± 0.0049 in high concentration > 0.2260 ± 0.0048 in low concentration > 0.1987 ± 0.0042 before treatment; **Figure 4B**). Although the difference was not obvious visually, we found that the rescuing effect of high CID concentration treatment was better than that of low concentration, indicated by their quantification. All the differences were significant, with P-values less than 0.0001.

In addition, the frequency distribution plots of the treated Rab7$^{V162M/V162M}$ homozygous MEFs also demonstrated the rescuing effect. There was a higher percentage of relatively smaller (area <0.8 μm^2), shorter (aspect ratio <3), and unbranched mitochondria (#of branch junctions =0) before treatments. In comparison, there was a higher ratio of relatively larger (area > 0.8 μm^2), longer (aspect ratio>3), and branched mitochondria (# of branched junctions ≥1) after treatments (**Figure 3C, 4C**).

The negative control for both CID and Mdivi-1 treatments was DMSO, a common solvent for drugs. The mitochondria for DMSO treatment only were fragmented (**Figure 3A**, middle panel). Their mean area (0.7186 ± 0.0048), aspect ratio (2.5362 ± 0.0088), the number of branch junctions (0.1616 ± 0.0038), and their frequency distribution were similar to that of untreated Rab7$^{V162M/V162M}$ homozygous mitochondria (**Figure 3B, 3C**, middle panels). The DMSO data indicated that only adding the solvent did not cause any changed to mitochondria morphology and that the inhibitors were responsible for the rescuing effect.

Discussion

In the present study, we explored mitochondrial fragmentation and its possible mechanism in CMT2B. Using Rab7^{V162M} knock-in mouse model and rescuing treatments, we confirmed fragmentation in CMT2B fibroblasts and showed that mutant Rab7 was associated with increased DRP1 activity, leading to mitochondrial fragmentation.

CMT2B is an inherited autosomal dominant disease. Recent studies have shown that mutations in the Rab7 small GTPase led to CMT2B (Cogli et al., 2009; Kwon et al., 1995; Meggouh et al., 2006; Verhoeven et al., 2003). Rab7 plays a vital role in regulating endocytic pathways and endocytic trafficking (Bucci et al., 2000; Stenmark & Gillooly, 2001; Stenmark & Olkkonen, 2001). By recycling between an active, GTP-bound form and an inactive, GDP-bound form, Rab7 regulated aggregation and fusion of late endosomes/lysosomes (Bucci et al., 2000). The CMT2B-associated Rab7 mutations may loosen the regulation of the GDP to GTP exchange by Rab7 GEF (McCray et al., 2009; Saxena et al., 2005; Spinosa et al., 2008; Zhang et al., 2013). In addition, mutant Rab7 predominantly affects peripheral sensory neurons in the patients (Ponomareva et al., 2016; Suter & Scherer, 2003). One plausible explanation is that these neurons tend to have extremely long axons (Bucci et al., 2012; Cogli et al., 2009; Liu & Wu, 2017). Given that the wellbeing of mitochondria is also highly critical for maintaining the structure and function of these long axons (Cogli et al., 2009; Schiavon et al., 2021; Zhang et al., 2013; Zhao et al., 2012; Zhou et al., 2019). Thus, it is not surprising that alterations in mitochondrial motility, morphology, and function are intimately associated with CMT peripheral neuropathy (Cantarero et al., 2021). Therefore, our group is interested in studying the mutant Rab7 effect on the CMT2B mitochondria.

Recent studies have shown that the Rab7 mutations led to the enlargement of mitochondria (Cioni et al., 2019) or shown that Rab7 mutations caused a decreased rate of mitochondrial fission (Wong et al., 2018). These studies utilized transient overexpression of Rab7 constructs in immortal

cell lines (Wong et al., 2018) or retinal ganglion cells (Cioni et al., 2019) to study mitochondria dynamics. However, this method has two potential problems: First, the immortal cells and the retinal ganglion cells are not physiologically relevant to CMT2B. CMT2B is peripheral neuropathy that mainly affects the patient peripheral neurons. The immortal cell lines (such as Hela cells) and the retinal ganglion cells were physiologically distinct from the peripheral neurons. In addition, immortal cell lines such as cancer cells usually underwent some permanent changes in their cellular pathways, which might change their gene expression and make them different from the normal cells. Secondly, we cannot control the ratio of wild-type and mutant Rab7 proteins in this method. Given that CMT2B is an autosomal dominant disease, the genotype for almost all the CMT2B patients is Rab7 heterozygote, containing only one mutant Rab7 allele. Therefore, the ratio between wild-type and mutant Rab7 is exactly 1:1. However, in the transient overexpression model, the enhanced GFP-labeled wild type and mutant Rab7 cDNAs were cloned into a vector, and then the cells were transfected with the plasmid (Pan et al., 2020). Therefore, the artificial Rab7 gene and the endogenous Rab7 gene co-existed and were under different promoters. As a result, it is impossible to control the ratio of artificial and endogenous Rab7 to mimic the genome in CMT2B patients. In our experiments, we obtained the fibroblasts from the abdominal area of mouse embryo, which were primary cells relevant to CMT2B. In addition, we used a $Rab7^{V162M}$ knock-in mouse model, which directly edits the genome and mimics the ratio of wild-type and mutant Rab7 in CMT2B patients.

After confirming the mitochondrial fragmentation in CMT2B, we were interested in how Rab7 mutations in CMT2B led to mitochondria fragmentation. Previous studies have shown that the knocking down of Rab7 decreased DRP1 phosphorylation at the Ser616 domain, leading to decreased DRP1 activity (Pan et al., 2020). These studies indicated the ability of Rab7 to regulate

the DRP1 activity for mitochondria dynamics. Therefore, we hypothesized that the CMT2B mutations increased Rab7 activity, leading to enhanced DRP1 activity, which induced extremely mitochondrial fragmentation.

If the enhanced DRP1 activity in CMT2B led to excessive mitochondrial fragmentation, a Drp1 inhibitor should mitigate mitochondrial fragmentation and thus rescue mitochondria morphology. We found that the Mdivi-1 treatment for $Rab7^{V162M/V162M}$ homozygote mitochondria recovered their size, shape, and network, indicated by their mean area, aspect ratio, and the number of branch junctions (Figure 3A, B). In addition, if mutant Rab7 in CMT2B increased the DRP1 activity, a Rab7 inhibitor should decrease the DRP1 activity, also leading to less mitochondrial fragmentation. We found that both high and low concentrations of CID treatment for $Rab7^{V162M/V162M}$ homozygous mitochondria successfully mitigated mitochondrial fragmentation and rescued mitochondrial morphology, indicated by their increased mean area, aspect ratio, and the number of branch junctions per mitochondrion (Figure 4A, B). The results of CID and Mdivi-1 treatments provided evidence to support our hypothesis that the CMT2B mutations increased Rab7 activity, leading to enhanced DRP1 activity, and mitochondrial fragmentation is a consequence of enhanced DRP1 activity.

As mentioned earlier, the genotypes for most CMT2B patients were Rab7 heterozygote, given that CMT2B is an autosomal dominant disease. However, both the Mdivi-1 and CID in our study were used to treat Rab7 homozygous MEFs. The reason was that the difference between wild-type and $Rab7^{V162M/V162M}$ homozygote was more significant than that between wild-type and $Rab7^{V162M/+}$ heterozygote. We chose the homozygote because their rescuing effect after treatment was more prominent. In addition, DMSO, the solvent for the drugs, was the negative control group. However, the three characteristics for DMSO and homozygote also had significant differences.

One plausible explanation is that the samples involved in each group are over 20,000. Such a large sample size made even a tiny difference statistically significant. Our focus here is the comparison before and after treatment.

Furthermore, there are two possible pathways: Mutant Rab7 can increase DRP1 activity either by increasing total DRP1 protein expression or by increasing DRP1 phosphorylation, or both. Further studies should focus on how mutant Rab7 increased Drp1 activity. We can use western blot to assay the DRP1 and phosphorylated DRP1 expression level in pathologic genotypes to test mutant Rab7 effect on DRP1.

In conclusion, our results presented the excessive mitochondria fragmentation in the CMT2B-associated mutant mouse embryonic fibroblasts. Furthermore, we demonstrated that CMT2B mutation(s) increased the Rab7 activity, leading to enhanced Drp1 activity. As a result, the mitochondria became extremely fragmented in CMT2B.

The material in this thesis is currently being prepared for submission for publication. Hu, Mingzheng; Wu, Chengbiao; Gu, Yingli. The thesis author was the primary author of this material.

Works Cited

Auer-Grumbach, M., De Jonghe, P., Verhoeven, K., Timmerman, V., Wagner, K., Hartung, H.-P., & Nicholson, G. A. (2003). Autosomal Dominant Inherited Neuropathies With Prominent Sensory Loss and Mutilations: A Review. *Archives of Neurology*, *60*(3), 329-334. https://doi.org/10.1001/archneur.60.3.329

Auer-Grumbach, M., De Jonghe, P., Wagner, K., Verhoeven, K., Hartung, H. P., & Timmerman, V. (2000). Phenotype-genotype correlations in a CMT2B family with refined 3q13-q22 locus. *Neurology*, *55*(10), 1552-1557. https://doi.org/10.1212/wnl.55.10.1552

Auer-Grumbach, M., Wagner, K., Timmerman, V., De Jonghe, P., & Hartung, H. P. (2000). Ulcero-mutilating neuropathy in an Austrian kinship without linkage to hereditary motor and sensory neuropathy IIB and hereditary sensory neuropathy I loci. *Neurology*, *54*(1), 45-52. https://doi.org/10.1212/wnl.54.1.45

Baloh, R. H., Schmidt, R. E., Pestronk, A., & Milbrandt, J. (2007). Altered Axonal Mitochondrial Transport in the Pathogenesis of Charcot-Marie-Tooth Disease from Mitofusin 2 Mutations. *The Journal of Neuroscience*, *27*(2), 422-430. https://doi.org/10.1523/jneurosci.4798-06.2007

Barisic, N., Claeys, K. G., Sirotković-Skerlev, M., Löfgren, A., Nelis, E., De Jonghe, P., & Timmerman, V. (2008). Charcot-Marie-Tooth Disease: A Clinico-genetic Confrontation. *Annals of Human Genetics*, *72*(3), 416-441. https://doi.org/https://doi.org/10.1111/j.1469-1809.2007.00412.x

Bennett, C. L., & Chance, P. F. (2001). Molecular pathogenesis of hereditary motor, sensory and autonomic neuropathies. *Current Opinion in Neurology*, *14*(5), 621-627. https://journals.lww.com/coneurology/Fulltext/2001/10000/Molecular_pathogenesis_of_hereditary_motor,.11.aspx

Bucci, C., Bakke, O., & Progida, C. (2012). Charcot-Marie-Tooth disease and intracellular traffic. *Prog Neurobiol*, *99*(3), 191-225. https://doi.org/10.1016/j.pneurobio.2012.03.003

Bucci, C., & De Luca, M. (2012). Molecular basis of Charcot-Marie-Tooth type 2B disease. *Biochem Soc Trans*, *40*(6), 1368-1372. https://doi.org/10.1042/BST20120197

Bucci, C., Thomsen, P., Nicoziani, P., McCarthy, J., & van Deurs, B. (2000). Rab7: a key to lysosome biogenesis. *Mol Biol Cell*, *11*(2), 467-480. https://doi.org/10.1091/mbc.11.2.467

Cantarero, L., Juarez-Escoto, E., Civera-Tregon, A., Rodriguez-Sanz, M., Roldan, M., Benitez, R., Hoenicka, J., & Palau, F. (2021). Mitochondria-lysosome membrane contacts are defective in GDAP1-related Charcot-Marie-Tooth disease. *Hum Mol Genet*, *29*(22), 3589-3605. https://doi.org/10.1093/hmg/ddaa243

Chaudhry, A., Shi, R., & Luciani, D. S. (2020). A pipeline for multidimensional confocal analysis of mitochondrial morphology, function, and dynamics in pancreatic β-cells. *American Journal of Physiology-Endocrinology and Metabolism*, *318*(2), E87-E101. https://doi.org/10.1152/ajpendo.00457.2019

Cioni, J.-M., Lin, J. Q., Holtermann, A. V., Koppers, M., Jakobs, M. A. H., Azizi, A., Turner-Bridger, B., Shigeoka, T., Franze, K., Harris, W. A., & Holt, C. E. (2019). Late Endosomes Act as mRNA Translation Platforms and Sustain Mitochondria in Axons. *Cell*, *176*(1), 56-72.e15. https://doi.org/https://doi.org/10.1016/j.cell.2018.11.030

Cogli, L., Piro, F., & Bucci, C. (2009). Rab7 and the CMT2B disease. *Biochem Soc Trans*, *37*(Pt 5), 1027-1031. https://doi.org/10.1042/BST0371027

Cogli, L., Progida, C., Lecci, R., Bramato, R., Kruttgen, A., & Bucci, C. (2010). CMT2B-associated Rab7 mutants inhibit neurite outgrowth. *Acta Neuropathol*, *120*(4), 491-501. https://doi.org/10.1007/s00401-010-0696-8

Cogli, L., Progida, C., Thomas, C. L., Spencer-Dene, B., Donno, C., Schiavo, G., & Bucci, C. (2013). Charcot-Marie-Tooth type 2B disease-causing RAB7A mutant proteins show altered interaction with the neuronal intermediate filament peripherin. *Acta Neuropathol*, *125*(2), 257-272. https://doi.org/10.1007/s00401-012-1063-8

Colecchia, D., Stasi, M., Leonardi, M., Manganelli, F., Nolano, M., Veneziani, B. M., Santoro, L., Eskelinen, E. L., Chiariello, M., & Bucci, C. (2018). Alterations of autophagy in the peripheral neuropathy Charcot-Marie-Tooth type 2B. *Autophagy*, *14*(6), 930-941. https://doi.org/10.1080/15548627.2017.1388475

Fenton, A. R., Jongens, T. A., & Holzbaur, E. L. F. (2021). Mitochondrial dynamics: Shaping and remodeling an organelle network. *Curr Opin Cell Biol*, *68*, 28-36. https://doi.org/10.1016/j.ceb.2020.08.014

Filadi, R., Pendin, D., & Pizzo, P. (2018). Mitofusin 2: from functions to disease. *Cell Death Dis*, *9*(3), 330. https://doi.org/10.1038/s41419-017-0023-6

Franco, A., Dang, X., Walton, E. K., Ho, J. N., Zablocka, B., Ly, C., Miller, T. M., Baloh, R. H., Shy, M. E., Yoo, A. S., & Dorn, G. W., 2nd. (2020). Burst mitofusin activation reverses neuromuscular dysfunction in murine CMT2A. *Elife*, *9*. https://doi.org/10.7554/eLife.61119

Galvan, D. L., Long, J., Green, N., Chang, B. H., Lin, J. S., Schumacker, P., Truong, L. D., Overbeek, P., & Danesh, F. R. (2019). Drp1S600 phosphorylation regulates mitochondrial fission and progression of nephropathy in diabetic mice. *J Clin Invest*, *129*(7), 2807-2823. https://doi.org/10.1172/JCI127277

Houlden, H., King, R. H. M., Muddle, J. R., Warner, T. T., Reilly, M. M., Orrell, R. W., & Ginsberg, L. (2004). A novel RAB7 mutation associated with ulcero-mutilating

neuropathy. *Annals of Neurology*, *56*(4), 586-590. https://doi.org/https://doi.org/10.1002/ana.20281

Kim, D. I., Lee, K. H., Gabr, A. A., Choi, G. E., Kim, J. S., Ko, S. H., & Han, H. J. (2016). Aβ-Induced Drp1 phosphorylation through Akt activation promotes excessive mitochondrial fission leading to neuronal apoptosis. *Biochimica et Biophysica Acta (BBA) - Molecular Cell Research*, *1863*(11), 2820-2834. https://doi.org/https://doi.org/10.1016/j.bbamcr.2016.09.003

Kwon, J. M., Elliott, J. L., Yee, W. C., Ivanovich, J., Scavarda, N. J., Moolsintong, P. J., & Goodfellow, P. J. (1995). Assignment of a second Charcot-Marie-Tooth type II locus to chromosome 3q. *Am J Hum Genet*, *57*(4), 853-858. https://www.ncbi.nlm.nih.gov/pubmed/7573046

Li, Y.-J., Cao, Y.-L., Feng, J.-X., Qi, Y., Meng, S., Yang, J.-F., Zhong, Y.-T., Kang, S., Chen, X., Lan, L., Luo, L., Yu, B., Chen, S., Chan, D. C., Hu, J., & Gao, S. (2019). Structural insights of human mitofusin-2 into mitochondrial fusion and CMT2A onset. *Nature Communications*, *10*(1), 4914. https://doi.org/10.1038/s41467-019-12912-0

Liu, H., & Wu, C. (2017). Charcot Marie Tooth 2B Peripheral Sensory Neuropathy: How Rab7 Mutations Impact NGF Signaling? *International Journal of Molecular Sciences*, *18*(2), 324. https://www.mdpi.com/1422-0067/18/2/324

Manganelli, F., Pisciotta, C., Provitera, V., Taioli, F., Iodice, R., Topa, A., Fabrizi, G. M., Nolano, M., & Santoro, L. (2012). Autonomic nervous system involvement in a new CMT2B family. *J Peripher Nerv Syst*, *17*(3), 361-364. https://doi.org/10.1111/j.1529-8027.2012.00415.x

McCray, B. A., Skordalakes, E., & Taylor, J. P. (2009). Disease mutations in Rab7 result in unregulated nucleotide exchange and inappropriate activation. *Human Molecular Genetics*, *19*(6), 1033-1047. https://doi.org/10.1093/hmg/ddp567

Meggouh, F., Bienfait, H. M. E., Weterman, M. A. J., de Visser, M., & Baas, F. (2006). Charcot-Marie-Tooth disease due to a de novo mutation of the RAB7 gene. *Neurology*, *67*(8), 1476-1478. https://doi.org/10.1212/01.wnl.0000240068.21499.f5

Pan, Z.-N., Pan, M.-H., Sun, M.-H., Li, X.-H., Zhang, Y., & Sun, S.-C. (2020). RAB7 GTPase regulates actin dynamics for DRP1-mediated mitochondria function and spindle migration in mouse oocyte meiosis. *The FASEB Journal*, *34*(7), 9615-9627. https://doi.org/https://doi.org/10.1096/fj.201903013R

Ponomareva, O. Y., Eliceiri, K. W., & Halloran, M. C. (2016). Charcot-Marie-Tooth 2b associated Rab7 mutations cause axon growth and guidance defects during vertebrate sensory neuron development. *Neural Development*, *11*(1), 2. https://doi.org/10.1186/s13064-016-0058-x

Roe, A. J., & Qi, X. (2018). Drp1 phosphorylation by MAPK1 causes mitochondrial dysfunction in cell culture model of Huntington's disease. *Biochemical and Biophysical Research Communications*, *496*(2), 706-711. https://doi.org/https://doi.org/10.1016/j.bbrc.2018.01.114

Rosales, K. R., Peralta, E. R., Guenther, G. G., Wong, S. Y., & Edinger, A. L. (2009). Rab7 Activation by Growth Factor Withdrawal Contributes to the Induction of Apoptosis. *Molecular Biology of the Cell*, *20*(12), 2831-2840. https://doi.org/10.1091/mbc.e08-09-0911

Saveri, P., De Luca, M., Nisi, V., Pisciotta, C., Romano, R., Piscosquito, G., Reilly, M. M., Polke, J. M., Cavallaro, T., Fabrizi, G. M., Fossa, P., Cichero, E., Lombardi, R., Lauria, G., Magri, S., Taroni, F., Pareyson, D., & Bucci, C. (2020). Charcot-Marie-Tooth Type 2B: A New Phenotype Associated with a Novel RAB7A Mutation and Inhibited EGFR Degradation. *Cells*, *9*(4), 1028. https://www.mdpi.com/2073-4409/9/4/1028

Saxena, S., Bucci, C., Weis, J., & Kruttgen, A. (2005). The small GTPase Rab7 controls the endosomal trafficking and neuritogenic signaling of the nerve growth factor receptor TrkA. *J Neurosci*, *25*(47), 10930-10940. https://doi.org/10.1523/JNEUROSCI.2029-05.2005

Schiavon, C. R., Shadel, G. S., & Manor, U. (2021). Impaired Mitochondrial Mobility in Charcot-Marie-Tooth Disease [Perspective]. *Frontiers in Cell and Developmental Biology*, *9*(35). https://doi.org/10.3389/fcell.2021.624823

Spinosa, M. R., Progida, C., De Luca, A., Colucci, A. M., Alifano, P., & Bucci, C. (2008). Functional characterization of Rab7 mutant proteins associated with Charcot-Marie-Tooth type 2B disease. *J Neurosci*, *28*(7), 1640-1648. https://doi.org/10.1523/JNEUROSCI.3677-07.2008

Stenmark, H., & Gillooly, D. J. (2001). Intracellular trafficking and turnover of phosphatidylinositol 3-phosphate. *Seminars in Cell & Developmental Biology*, *12*(2), 193-199. https://doi.org/https://doi.org/10.1006/scdb.2000.0236

Stenmark, H., & Olkkonen, V. M. (2001). The Rab GTPase family. *Genome Biol*, *2*(5), REVIEWS3007. https://doi.org/10.1186/gb-2001-2-5-reviews3007

Suter, U., & Scherer, S. S. (2003). Disease mechanisms in inherited neuropathies. *Nat Rev Neurosci*, *4*(9), 714-726. https://doi.org/10.1038/nrn1196

Valente, A. J., Maddalena, L. A., Robb, E. L., Moradi, F., & Stuart, J. A. (2017). A simple ImageJ macro tool for analyzing mitochondrial network morphology in mammalian cell culture. *Acta Histochem*, *119*(3), 315-326. https://doi.org/10.1016/j.acthis.2017.03.001

Verhoeven, K., De Jonghe, P., Coen, K., Verpoorten, N., Auer-Grumbach, M., Kwon, J. M., FitzPatrick, D., Schmedding, E., De Vriendt, E., Jacobs, A., Van Gerwen, V., Wagner,

K., Hartung, H. P., & Timmerman, V. (2003). Mutations in the small GTP-ase late endosomal protein RAB7 cause Charcot-Marie-Tooth type 2B neuropathy. *Am J Hum Genet*, *72*(3), 722-727. https://doi.org/10.1086/367847

Wang, X., Han, C., Liu, W., Wang, P., & Zhang, X. (2014). A novel RAB7 mutation in a Chinese family with Charcot–Marie–Tooth type 2B disease. *Gene*, *534*(2), 431-434. https://doi.org/https://doi.org/10.1016/j.gene.2013.10.023

Wong, Y. C., Kim, S., Peng, W., & Krainc, D. (2019). Regulation and Function of Mitochondria–Lysosome Membrane Contact Sites in Cellular Homeostasis. *Trends in Cell Biology*, *29*(6), 500-513. https://doi.org/https://doi.org/10.1016/j.tcb.2019.02.004

Wong, Y. C., Peng, W., & Krainc, D. (2019). Lysosomal Regulation of Inter-mitochondrial Contact Fate and Motility in Charcot-Marie-Tooth Type 2. *Developmental Cell*, *50*(3), 339-354.e334. https://doi.org/https://doi.org/10.1016/j.devcel.2019.05.033

Wong, Y. C., Ysselstein, D., & Krainc, D. (2018). Mitochondria–lysosome contacts regulate mitochondrial fission via RAB7 GTP hydrolysis. *Nature*, *554*(7692), 382-386. https://doi.org/10.1038/nature25486

Zhang, K., Fishel Ben Kenan, R., Osakada, Y., Xu, W., Sinit, R. S., Chen, L., Zhao, X., Chen, J.-Y., Cui, B., & Wu, C. (2013). Defective Axonal Transport of Rab7 GTPase Results in Dysregulated Trophic Signaling. *The Journal of Neuroscience*, *33*(17), 7451-7462. https://doi.org/10.1523/jneurosci.4322-12.2013

Zhao, T., Huang, X., Han, L., Wang, X., Cheng, H., Zhao, Y., Chen, Q., Chen, J., Cheng, H., Xiao, R., & Zheng, M. (2012). Central Role of Mitofusin 2 in Autophagosome-Lysosome Fusion in Cardiomyocytes*. *Journal of Biological Chemistry*, *287*(28), 23615-23625. https://doi.org/https://doi.org/10.1074/jbc.M112.379164

Zhou, Y., Carmona, S., Muhammad, A., Bell, S., Landeros, J., Vazquez, M., Ho, R., Franco, A., Lu, B., Dorn, G. W., 2nd, Wang, S., Lutz, C. M., & Baloh, R. H. (2019). Restoring mitofusin balance prevents axonal degeneration in a Charcot-Marie-Tooth type 2A model. *J Clin Invest*, *129*(4), 1756-1771. https://doi.org/10.1172/jci124194